JGR Oceans

RESEARCH ARTICLE
10.1029/2021JC018112

Focusing and Defocusing of Tropical Cyclone Generated Waves by Ocean Current Refraction

Rui Sun[1], Ana B. Villas Bôas[1], Aneesh C. Subramanian[2], Bruce D. Cornuelle[1], Matthew R. Mazloff[1], Arthur J. Miller[1], Sabique Langodan[3], and Ibrahim Hoteit[3]

[1]Scripps Institution of Oceanography, La Jolla, CA, USA, [2]Department of Atmospheric and Oceanic Sciences, University of Colorado Boulder, Boulder, CO, USA, [3]Physical Sciences and Engineering Division, King Abdullah University of Science and Technology (KAUST), Thuwal, Saudi Arabia

Key Points:

- Altimeter data and WAVEWATCH III are used to quantify ocean current impacts on surface waves
- Coherent wave beams propagate from tropical cyclone eyewalls due to current-induced refraction
- Wave height structure is dominated by background currents, and not the cyclone induced currents

Supporting Information:

Supporting Information may be found in the online version of this article.

Correspondence to:

R. Sun,
rus043@ucsd.edu

Citation:

Sun, R., Villas Bôas, A. B., Subramanian, A. C., Cornuelle, B. D., Mazloff, M. R., Miller, A. J., et al. (2022). Focusing and defocusing of tropical cyclone generated waves by ocean current refraction. *Journal of Geophysical Research: Oceans*, *127*, e2021JC018112. https://doi.org/10.1029/2021JC018112

Received 5 NOV 2021
Accepted 4 JAN 2022

Author Contributions:

Conceptualization: Ana B. Villas Bôas
Funding acquisition: Bruce D. Cornuelle, Matthew R. Mazloff, Arthur J. Miller, Ibrahim Hoteit
Investigation: Ana B. Villas Bôas, Aneesh C. Subramanian, Matthew R. Mazloff, Arthur J. Miller, Sabique Langodan, Ibrahim Hoteit
Methodology: Ana B. Villas Bôas, Bruce D. Cornuelle, Matthew R. Mazloff, Sabique Langodan
Software: Sabique Langodan
Supervision: Bruce D. Cornuelle, Matthew R. Mazloff, Arthur J. Miller, Ibrahim Hoteit
Writing – original draft: Ana B. Villas Bôas, Aneesh C. Subramanian
Writing – review & editing: Ana B. Villas Bôas, Aneesh C. Subramanian, Bruce D. Cornuelle, Matthew R. Mazloff, Arthur J. Miller, Sabique Langodan, Ibrahim Hoteit

Abstract Waves generated by tropical cyclones can have devastating effects on coastal regions. However, the role of ocean currents in modifying wave amplitudes, wavelengths, and directions is commonly overlooked in wave forecasts, despite the fact that these interactions can lead to extreme wave conditions. Here, we use satellite observations and wave modeling to quantify the effects of ocean currents on the surface waves generated during a tropical cyclone event in the Arabian Sea. As a case study, this paper documents beams of wave heights originating from the eyewall of a tropical cyclone caused by current-induced refraction. Alternating regions of high and low wave heights in the model simulations are consistent with observations and extend for thousands of kilometers all the way to 100 m isobath. Our results highlight the importance of accounting for wave refraction by currents in order to accurately predict the impact of tropical cyclone generated waves on coastal regions.

Plain Language Summary Waves generated by tropical cyclones can have devastating effects on coastal regions. Ocean currents can modify wave heights and lead to extreme wave conditions. Here, we use satellite observations and wave modeling to quantify the effects of ocean currents on the waves during a tropical cyclone event in the Arabian Sea. In this paper, we documented the coherent beams of wave heights originating from the "center" of a tropical cyclone caused by current-induced effects. Alternating regions of high and low wave heights in the model simulations are consistent with observations and extend for thousands of kilometers all the way to 100 m isobath. Our results highlight the importance of accounting for the currents in order to accurately predict the impact of tropical cyclone generated waves on coastal regions.

1. Introduction

Ocean surface waves mediate exchanges of momentum and energy across the air–sea interface. Thus, representing waves in weather and climate models is crucial for improving predictive skill (Cavaleri et al., 2012; Villas Bôas et al., 2019). Moreover, surface waves are an important driver of beach erosion, pollutant transport, and coastal flooding; hence understanding the evolution and propagation of surface waves and accurately modeling them has profound implications for both the coastal and global communities (Munk & Traylor, 1947).

Surface waves are generated by the wind, and extreme wind events, such as tropical cyclones, can produce extreme waves. Waves are affected by ocean currents via wave–current interactions, which modify their amplitude, wavelength, and direction. Recent numerical modeling studies have shown that the spatial variability of significant wave height H_s (the average of the highest one-third of the wave heights) at scales between 10 and 100 km is governed by the gradients in ocean currents (Ardhuin et al., 2017; Marechal & Ardhuin, 2021; Romero et al., 2020; Villas Bôas et al., 2020). Despite the limited spatial sampling of present satellite altimeters, novel signal processing techniques have provided observational evidence that supports these numerical results (Quilfen & Chapron, 2019; Quilfen et al., 2018).

In the context of tropical cyclones, several studies have explored the effects of currents on surface waves (Abolfazli et al., 2020; Chen et al., 2013; Drost et al., 2017; Fan, Ginis, & Hara, 2009; Fan, Ginis, Hara, Wright, & Walsh, 2009; Hegermiller et al., 2019; Holthuijsen & Tolman, 1991; Liu et al., 2017; Mogensen et al., 2017; Olabarrieta et al., 2012; Prakash & Pant, 2020; Warner et al., 2010). For example, Holthuijsen and Tolman (1991) performed a theoretical study on the interaction between a Gulf Stream eddy and ocean waves in swell and storm conditions. In their study, the wave model captured current-induced wave refractions that led to considerable

variation in significant wave height. In addition, Fan, Ginis, and Hara (2009) used a coupled wind–current-wave model to study processes at the air–sea interface under an idealized tropical cyclone scenario, and examined their effects on the wave field, wind stress, and ocean currents. Although the authors explored some aspects of wave–current interaction, their experiments only considered the effects of tropical cyclone generated currents. Recently, Hegermiller et al. (2019) studied wave–current interactions during Hurricane Matthew and found that the Gulf Stream modified the maximum coastal total water levels and resulted in the incident wave directions at the coast changing by up to 20°. However the Gulf Stream vorticity structure varies mostly cross-shore, and for the Hurricane Matthew case wave refraction was less significant in determining the spatial variability of the wave field. Here, in this case study, we report that far-field H_s from tropical cyclone generated waves can vary by meters due to refraction by background ocean currents. Building on the theoretical analysis by Holthuijsen and Tolman (1991), we validate model results with altimetry, providing observational evidence that tropical cyclone driven waves can have H_s variability of meters due to wave–current interactions.

The present study examines the surface wave field during Cyclone Mekunu in the Arabian Sea from a numerical modeling perspective and validates the results with satellite altimetry observations. We show how surface waves propagating away from the eyewall of a tropical cyclone have current-induced variations in H_s of up to 2 m within scales of hundreds of kilometers. The Arabian Sea is chosen because the tropical cyclones forming there often lead to considerable destruction and loss of life due to inundations (Dube et al., 1997; Evan & Camargo, 2011; Evan et al., 2011). In addition, continued anthropogenic forcing is likely to further amplify the risk of cyclones in the Arabian Sea and increase socioeconomic implications for coastal communities in that region (Murakami et al., 2017).

The rest of the paper is organized as follows. We first introduce the design of our numerical experiments with realistic currents, without currents, and with spatially smoothed currents. Then the results from the numerical simulations are presented and validated against altimeter data. The final section discusses the results and concludes this paper.

2. Experimental Design

In this case study, we used version 5.16 (WAVEWATCH III Development Group, 2016) of the WAVE-height, WATer depth and Current Hindcasting (WAVEWATCH III) third generation wave model (hereinafter, WW3) to investigate waves generated by Cyclone Mekunu, which was the strongest tropical cyclone in the north Indian Ocean in 2018. We selected this event because it overlaps with several passes from the Jason–3 and SARAL/AltiKa satellites in the Arabian Sea, providing cross-validation of our modeled H_s. We have run simulations during other cyclones in the Arabian Sea (see the Supporting Information S1) and the discussion presented here for Cyclone Mekunu applies for the other events as well.

The propagation of surface gravity waves in spectral wave models, such as WAVEWATCH III, is governed by the action balance equation:

$$\frac{\partial N}{\partial t} + \frac{1}{\cos\phi}\frac{\partial}{\partial \phi}\dot{\phi} N \cos\theta + \frac{\partial}{\partial \lambda}\dot{\lambda} N + \frac{\partial}{\partial k}\dot{k} N + \frac{\partial}{\partial \theta}\dot{\theta} N = S_{in} + S_{ds} + S_{nl}, \tag{1}$$

where $N = N(k, \theta; \phi, \lambda, t)$ is the action spectrum, k is the wavenumber, θ is the wave direction, ϕ is the latitude, λ is the longitude, t is the time, S_{in} is the input of action from the wind, S_{ds} is the dissipation, and S_{nl} represents nonlinear interactions. Additionally, the propagation velocities in physical and spectral space are given by:

$$\dot{\phi} = \frac{c_g \cos\theta + U_\phi}{R}, \tag{2}$$

$$\dot{\lambda} = \frac{c_g \sin\theta + U_\lambda}{R\cos\phi}, \tag{3}$$

$$\dot{k} = -\frac{\partial \sigma}{\partial d}\frac{\partial d}{\partial s} - \boldsymbol{k} \cdot \frac{\partial \boldsymbol{U}}{\partial s}, \tag{4}$$

$$\dot{\theta} = \dot{\theta}_{DG} - \frac{1}{k}\left[\frac{\partial \sigma}{\partial d}\frac{\partial d}{\partial m} + \boldsymbol{k} \cdot \frac{\partial \boldsymbol{U}}{\partial m}\right], \tag{5}$$

where $\boldsymbol{U}$ is the surface current, R is the Earth's radius, d is the water depth, s is a coordinate parallel to the wave direction, m is a coordinate perpendicular to the wave direction, $\dot{\theta}_{DG}$ is the apparent wave rotation due to the Earth's sphericity and water depth gradients, and $c_g = \partial\sigma/\partial k$ is the group speed, where σ is the intrinsic frequency given by the linear dispersion relation:

$$\sigma^2 = gk \tanh(kd). \tag{6}$$

From Equations 1–5 we see that currents and current gradients can impact the wave field by (a) changing the wind input S_{in} to account for the wind stress relative to the surface current; (b) changing the speed at which action is advected ($\boldsymbol{c_g} + \boldsymbol{U}$); (c) changing the wavenumber $\dot{k}$; (d) and finally changing the wave direction ($\dot{\theta}$), that is, causing wave refraction. The wave model setup used in the present manuscript includes all four effects, although our discussion will focus on the effects of refraction.

The model domain extends from 0° to 30.6°N and from 30 to 78°E with 0.075° spatial resolution in both latitude and longitude. The spectral grid of WW3 has 48 directions (7.5° resolution) and 32 frequencies exponentially spaced from 0.0343 to 1.1 Hz. The spatial and spectral resolution of the wave model used here are adequate to resolve the processed that focus on and increasing either spatial or spectral resolution does not impact our results (see Supporting Information S1 for more details). The wave spectra at the offshore boundary come from the global wave modeling system described by Rascle and Ardhuin (2013). The results that we analyze here span the period from 20–28 May, 2018 and we allowed the wave model to spin-up for 19 days from 01 May 2018. Our implementation of WW3 uses a global integration time step of 600 s, spatial advection time step of 60 s, spectral advection time step of 60 s, and minimum source term time step of 10 s. The recently proposed T475 parameterization is used with the wind input source term S_{in} in the present simulations (Alday et al., 2021). This aims to mitigate the error in the wave model when the wind speed is larger than 20 m s^{-1} in ERA5. In addition, we activated the PR3 option in WW3 to alleviate the Garden Sprinkler Effect (Booij & Holthuijsen, 1987) that can arise from coarse directional resolution by performing a spatial averaging (Tolman, 2002).

The wave model was forced with 10-m winds from ERA5 (Hersbach et al., 2020) and surface currents from the Global Ocean Forecasting System (GOFS) V3.1 HYCOM/NCODA 1/12° analysis (Chassignet et al., 2007; hereinafter, HYCOM). To evaluate the simulation performance, we compared the modeled H_s with along-track H_s measurements from the Jason-3 and SARAL/AltiKa altimeters. We use quality-controlled, unfiltered and not resampled, along-track H_s measurements provided by the Institut Français de Recherche pour l'Exploitation de la MER (Queffeulou & Croizé-Fillon, 2013; IFREMER; ftp://ftp.ifremer.fr/ifremer/cersat/products/swath/altimeters/waves/).

The following experiments were performed:

1. WAV.CUR: The hourly ERA5 winds and daily HYCOM currents were used to force the wave model.
2. WAV.WND: The hourly ERA5 winds were used to force the wave model. This experiment had no current forcing and it was aimed at investigating the effects of currents on the wave field.
3. WAV.CUR_STA: The hourly ERA5 winds and persistent HYCOM currents were used to drive the simulation. In this experiment, the HYCOM currents on the initial day (May 20) remain persistent through the simulation. Hence, the tropical cyclone-induced currents are not considered in this run.
4. WAV.CUR_LOW: The hourly ERA5 winds and spatially smoothed daily HYCOM currents were used to drive the simulation. The currents were averaged to 2.55° resolution in each direction (approximately 288 km). This run was performed to investigate the influence of current resolution.

3. Results

3.1. Modeled Significant Wave Height

The snapshots of sea level pressure and 10-m wind speed from ERA5 are presented in Figure 1 to illustrate the evolution of Cyclone Mekunu. The cyclone started forming on 20 May 2018 and then propagated to the northwest before making landfall on 26 May 2018 (Government of India, 2018). The corresponding snapshots of significant wave height H_s from WAV.CUR and WAV.WND are shown in Figure 2 (a–b and c–d, respectively). In both simulations, the highest wave heights are observed near the eyewall of the tropical cyclone, reaching a maximum of over 8 m on 24 May. In comparison with the results obtained from WAV.WND, alternating regions of high and

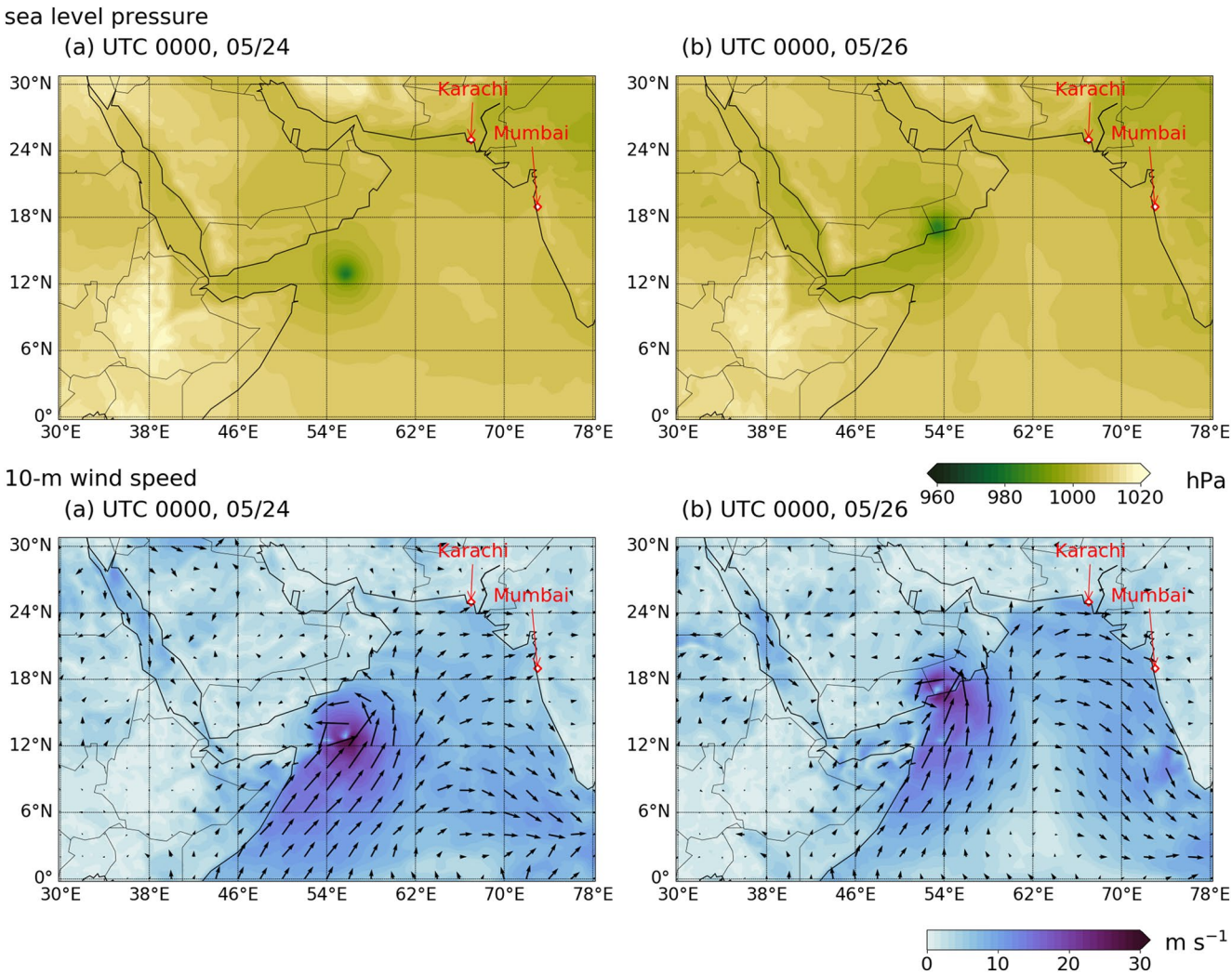

Figure 1. Snapshots of sea level pressure and wind speed during Cyclone Mekunu. Panels (a–b) show the contours of sea level pressure from ERA5; Panels (c–d) show 10-m wind speed from ERA5. The arrows in Panels (c–d) indicate the wind direction.

low H_s can be observed in WAV.CUR, particularly toward the end of the simulation (Figure 2b). These coherent "beams" of H_s extend from the eyewall of the tropical cyclone to the east, all the way to the 100 m isobath. As a consequence of wave current interactions, the significant wave heights reaching some locations near Mumbai and Karachi on 26th May are approximately 1 m higher in WAV.CUR than WAV.WND, with severe associated flood risk implications.

The differences of significant wave height H_s obtained from the simulations are shown in Figure 3. Compared with the wave field obtained from WAV.WND, alternating patterns of higher and lower waves are obtained from WAV.CUR, especially on 26th May (shown in Figure 3b). When the impact of the tropical cyclone induced currents is not considered (WAV.CUR_STA), the pattern in H_s observed in the far field is similar to WAV.CUR (shown in Figures 3c and 3d). In WAV.CUR_LOW the currents are spatially smoothed and the alternating patterns of H_s are much weaker compared with WAV.CUR and WAV.CUR_STA (shown in Figures 3e and 3f). On 24th May, H_s near the eyewall of the tropical cyclone (12°N, 56°E) in WAV.CUR and WAV.CUR_LOW is slightly smaller than WAV.WND, shown in Figures 3a and 3e, consistent with the results from Fan, Ginis, and Hara (2009) and Hegermiller et al. (2019). On the other hand, when the tropical cyclone induced currents are not considered (WAV.CUR_STA), there is no reduction in H_s near the eyewall. Since the goal of this paper is to

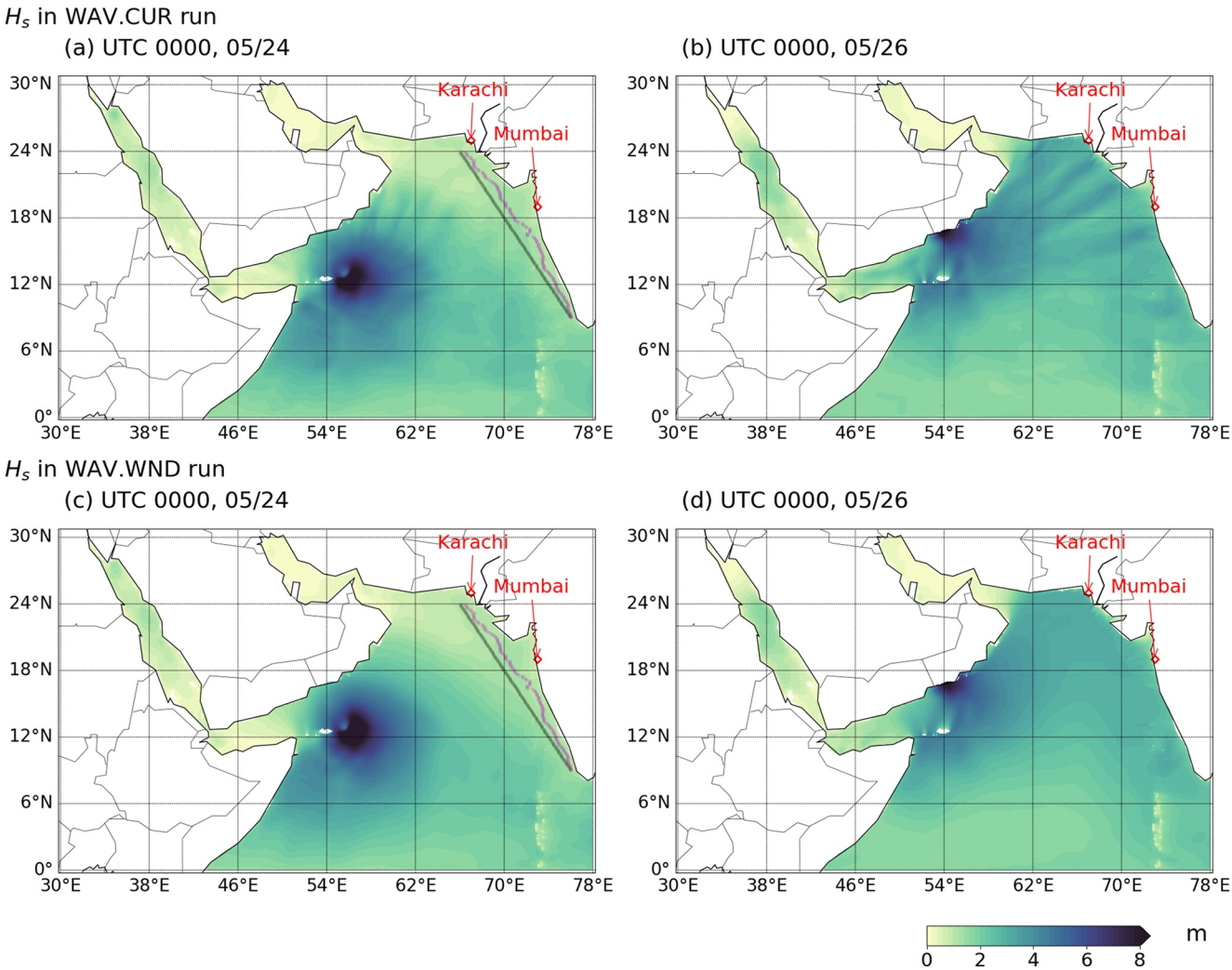

Figure 2. Snapshots of wave height H_s obtained from the simulations. Panels (a–b) show H_s from WAV.CUR run; Panels (c–d) show H_s from WAV.WND run. In Panels (a) and (c), the black lines indicate the location where the wave heights were sampled in Figure 6; the magenta lines indicate the 100 m isobath.

document the effect of the background currents, and thus we do not further detail the effects of tropical cyclone induced currents in this event.

3.2. Comparison With Satellite Altimetry

The significant wave height, H_s, obtained from all four experiments is compared with along-track altimeter data to validate our numerical results, as shown in Figure 4. In general, all model runs capture the large-scale spatial variability of H_s along the satellite tracks, especially in the near field of the cyclone (Figures 4a, 4b, and 4d). The differences between the simulation results and altimeter data may be because of the uncertainties of ERA5 wind, HYCOM currents, or initial condition. However, only the experiments that include full resolution current forcing (WAV.CUR and WAV.CUR_STA) properly capture the alternating high and low beams of H_s to the northeast of the cyclone that occur at scales of a few hundreds of kilometers (Figures 4b and 4d). Although there are some differences between WAV.CUR (blue) and WAV.CUR_STA (green), there is generally good agreement between the two runs to the northeast of the cyclone, suggesting that, in this case, cyclone-generated currents in HYCOM do not play a dominant role in producing the observed spatial variability in H_s. When the surface currents are spatially averaged (WAV.CUR_LOW, yellow), the impact of the currents on waves is much weaker, and the modeled

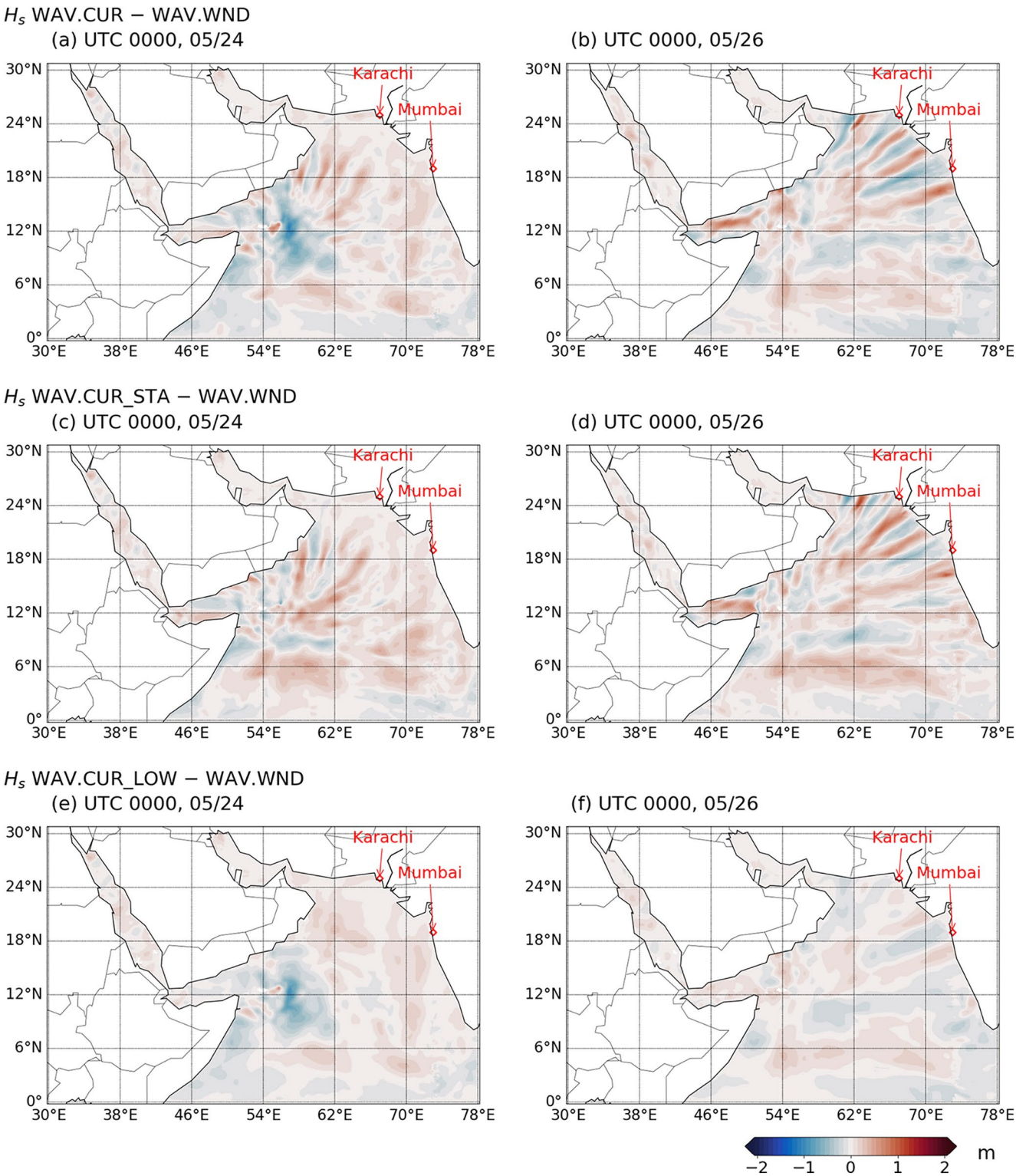

Figure 3. Difference of significant wave height H_s between the simulations. Panels (a–b) show H_s differences between WAV.CUR and WAV.WND; Panels (c–d) show H_s differences between WAV.CUR_STA and WAV.WND; Panels (e–f) show H_s differences between WAV.CUR_LOW and WAV.WND.

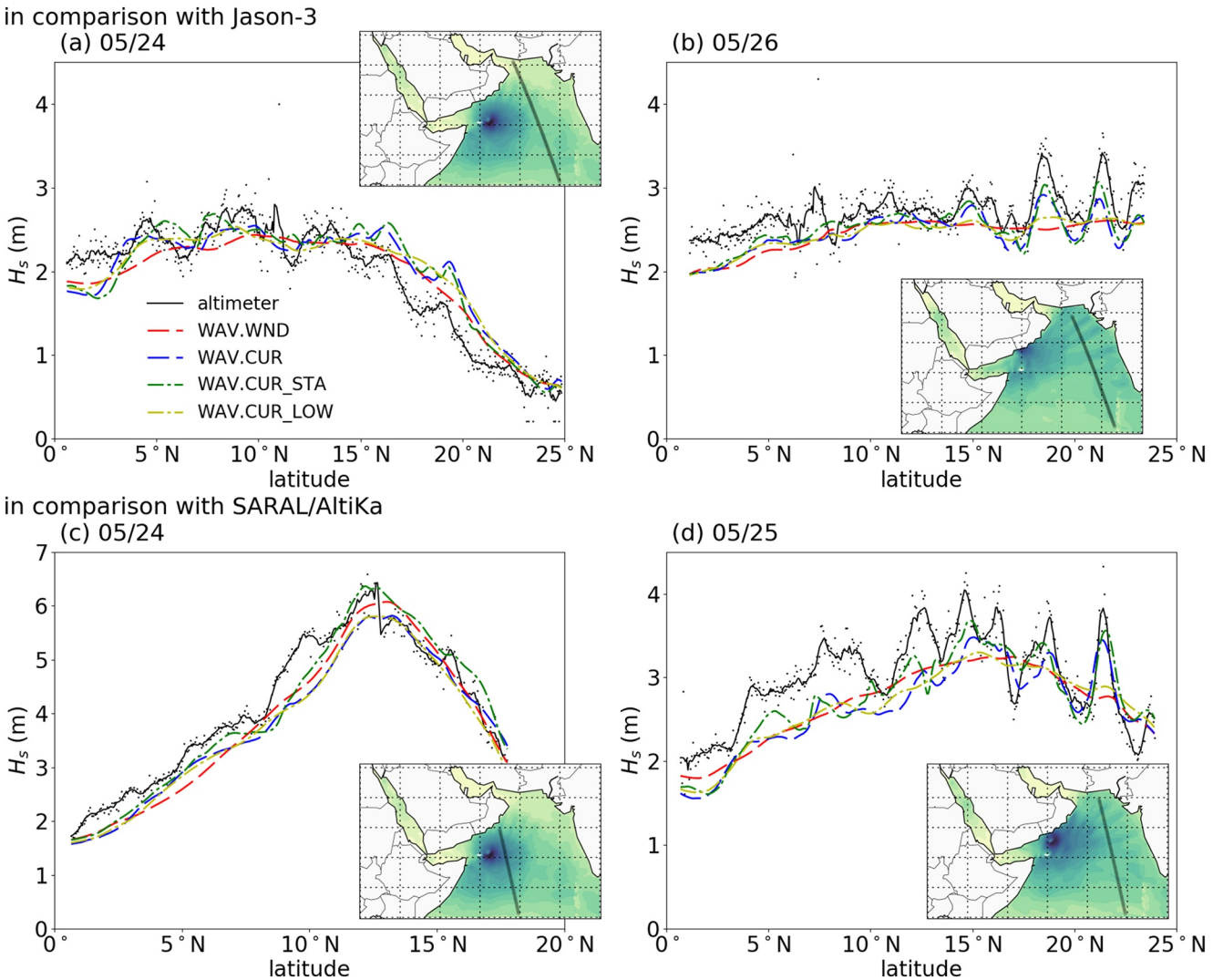

Figure 4. Comparison of significant wave height H_s between the simulations and altimeter data. Panels (a–b) show the comparison with JASON–3 for 24 and 26 May; Panels (c–d) show the comparison with SARAL for 24 and 25 May. Black dots correspond to the altimetry data, while in the solid black line the data are smoothed with a moving average of 0.5°. The altimeter tracks are highlighted in the inset figures. The scale of the filled contours in the insets is consistent with that in Figure 2.

H_s along altimetry tracks to the northeast of the cyclone is much smoother than observations (e.g., Figures 4b and 4d).

To quantify the differences between each model run, we compute the correlation coefficient between model and observation along each satellite track. Since this paper focuses on the effects of currents on waves, which are more pronounced at shorter spatial scales, the correlation coefficient was computed after removing the 600 km low-pass signal from each track, shown in Figure 5. We used the 600 km "box-car" low-pass filter because this distance is slightly larger than the distance between two consecutive beams in Figure 2. Using the high-pass filtered H_s highlights the correlation of H_s on scales shorter than 600 km, with correlation coefficients given in Table 1. The correlation coefficient values are dependent on the bandwidth of the filter. However, as long as the size of the filter is larger than the distance between high and low beams, the correlation coefficients of WAV.CUR and WAV.CUR_STA at three representative snapshots (Jason–3 05/24, 05/26, and AltiKa 05/25) are higher. This is because WAV.CUR and WAV.CUR_STA better capture the alternating patterns of H_s, shown in Figure 4. It is noted that if we select a larger window length (e.g., 700 or 800 km), the correlation coefficients are not significantly different.

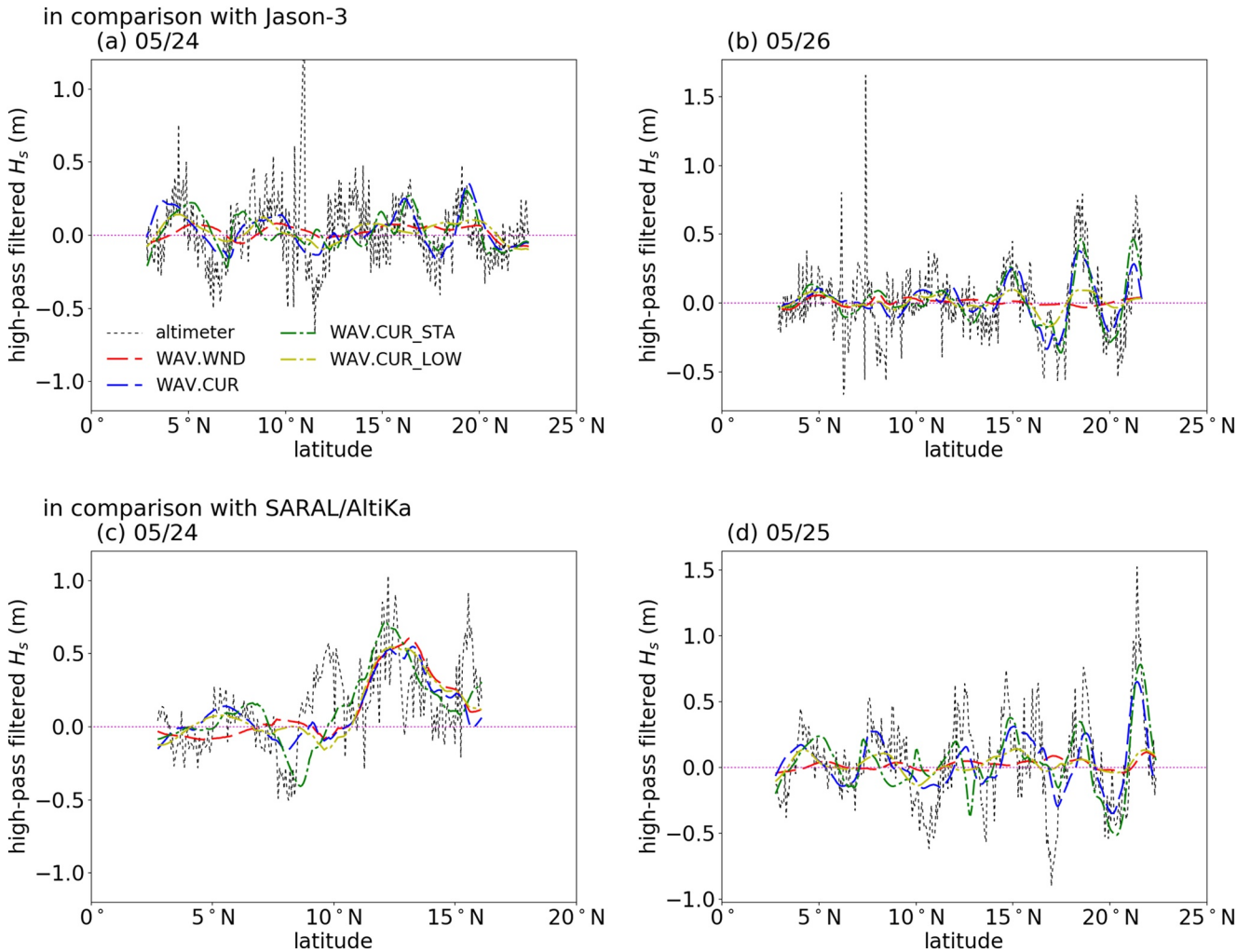

Figure 5. The wave height along the altimeter tracks after high-pass filtering scales longer than approximately 600 km. Panels (a–b) show the filtered data of JASON–3 for 24 and 26 May; Panels (c–d) show the filtered data of SARAL for 24 and 25 May.

3.3. Temporal Evolution of Significant Wave Height Along the Coast

The effects of currents in producing along-coast gradients in the wave field are emphasized by analyzing the temporal evolution of H_s from the four model runs in a quasi-alongshore section that closely follows the 100 m isobath between 9°N, 76°E and 24°N, 66°E (black line in Figure 2). The discrete high and low beams of H_s near the 100 m isobath of the east coast of the Arabian Sea that were observed in Figure 2 are shown in greater detail in Hovmöller diagrams (Figure 6). The significant wave heights in all simulations peak around 26 May; however, the spatial variability of H_s is notably different among the four panels. A remarkable feature revealed by Figure 6 is that when the effects of full resolution currents are taken into account (WAV.CUR and WAV.CUR_STA), the maximum wave heights near 17°N, 21°N, and 23°N are higher than those in WAV.WND by over 30%. Also, the time period with high wave heights (e.g., $H_s > 3$ m) lasts longer in WAV.CUR and WAV.CUR_STA than WAV.WND. In agreement with what was shown in the altimetry comparison in Figure 4, spatial gradients of H_s are much weaker in WAV.CUR_LOW than in the case of WAV.CUR and WAV.CUR_STA.

Table 1
Comparison of the Correlation Coefficients Between Modeled and Observed Significant Wave Height H_s Along Each Satellite Track After Removing the 600 km Low-Pass Signal

	Jason–3		SARAL/AltiKa	
	05/24	05/26	05/24	05/25
Experiment	Figure 2a	Figure 2b	Figure 2c	Figure 2d
WAV.WND	0.08	0.02	0.40	0.26
WAV.CUR	0.41	0.62	0.46	0.70
WAV.CUR_STA	0.28	0.63	0.52	0.56
WAV.CUR_LOW	0.27	0.51	0.40	0.51

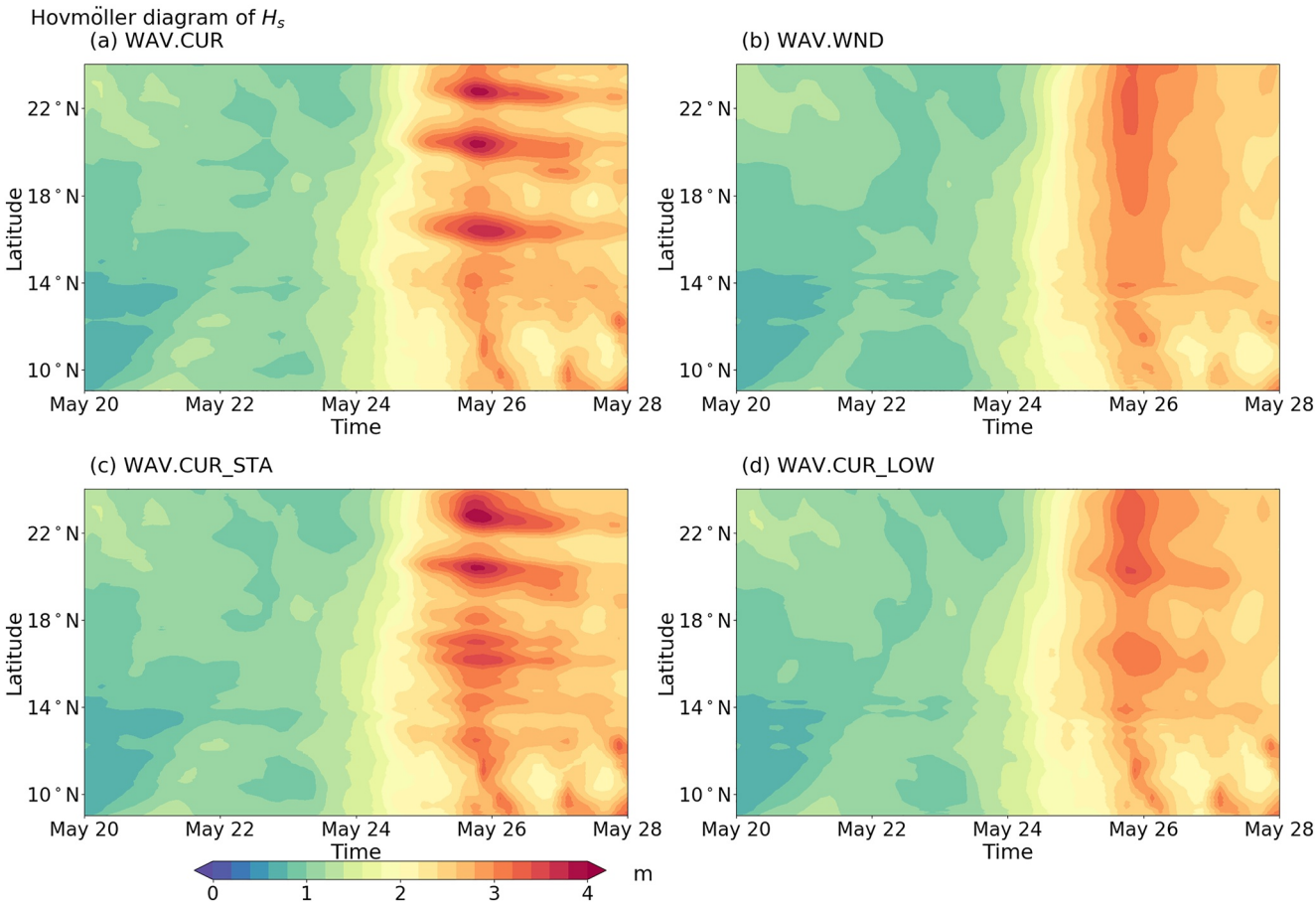

Figure 6. Spatial–temporal evolution of significant wave height H_s near the 100 m isobath of the east coast of the Arabian Sea. Panels (a–d) show the Hovmöller diagrams of WAV.CUR, WAV.WND, WAV.CUR_STA, and WAV.CUR_LOW, respectively.

3.4. Ray-Tracing Analysis

Surface currents can modify the amplitude, direction, and wavenumber of surface waves. In particular, current vorticity $\zeta = \partial v/\partial x - \partial u/\partial y$ causes wave rays to bend (i.e., refract) such that the wave propagation deviates from a straight line and, as a result, focusing and defocusing of wave energy occurs. Further validation of this mechanism was achieved by turning off the refraction term in WW3 (see Supporting Information S1), which resulted in smooth H_s fields that were nearly indistinguishable from the run without current forcing (on 26 May, the RMS difference is 0.10 m). However, for better visualization of the processes leading to the alternating high and low beams of significant wave height observed during Cyclone Mekunu we performed a ray-tracing analysis (Dysthe, 2001; Phillips, 1977; see Supporting Information S1 for details) using a surface current snapshot from 24 May and a wave period of 10.2 s, which is the peak period near the eyewall of the tropical cyclone (Figure 7b). We propagated 61 equally spaced rays starting from the eyewall with initial directions ranging from 195° to 255° (propagating to the northeast), which roughly encompasses the range of peak directions observed in the model output (Figure 7a, red box).

Figure 8a shows that locations with high and low concentration of rays (black lines) are generally consistent with the alternating high (red) and low (blue) beams of significant wave height shown in the background as a colormap. The discrepancy between the theoretical ray-tracing analysis and WW3 model can be attributed to a number of reasons. First, the ray-tracing performed here only considers monochromatic waves radiating from the eyewall of the tropical cyclone. Here, we also only show the ray-tracing results for waves initially at the peak frequency in our WW3 simulations. Additionally, the ray-tracing analysis assumes that the background currents are stationary during the propagation of the waves. In comparison with WAV.CUR, ray-tracing performed using currents from 20 May (WAV.CUR_STA, Figure 8b) results in similar patterns of focusing and defocusing of rays despite some

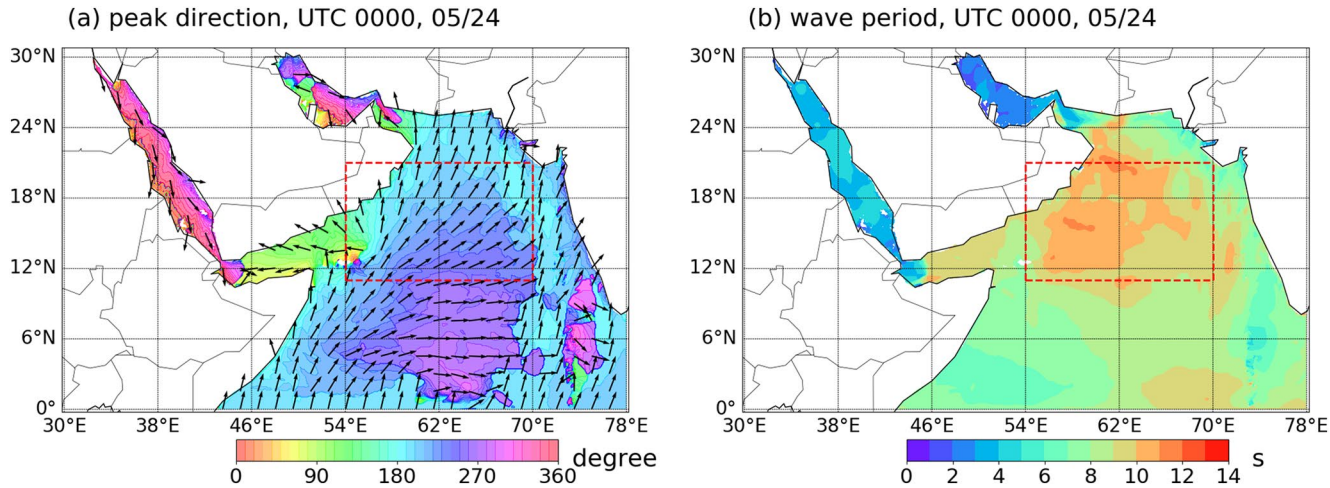

Figure 7. Peak direction and mean wave period obtained from WAV.CUR. Panel (a) shows the peak direction of the waves; Panel (b) shows the mean wave period in WAV.CUR. The arrows in Panel (a) denote the direction of the waves.

notable differences. When the currents are smoothed (WAV.CUR_LOW, Figure 8c), wave rays propagate in nearly straight lines and remain uniformly spaced.

Further interpretation of the ray paths is performed by considering the current vorticity field (Figure 9). Assuming the group speed of the waves, c_g, is much larger than the current speed implies the ray curvature, χ, is approximated by (Dysthe, 2001; Kenyon, 1971)

$$\chi = \zeta / c_g. \tag{7}$$

Thus, 10 s period waves propagating with a group speed of 8 m s^{-1} over a distance of 200 km in a current field with a mean vorticity of 2×10^{-5} s^{-1} would be deflected by approximately 29°. Equation 7 shows that positive (cyclonic) vorticity causes rays to bend to the left, while negative (anti-cyclonic) vorticity causes rays to bend to the right. In Figure 9b, we see a patch of positive vorticity (green) near 16°N, 62°E followed by a patch of negative vorticity (brown) just south of it. These regions of opposing vorticity cause the rays to diverge, resulting in an overall low concentration of rays to the northeast of 16°N, 62°E. This deflection of rays in opposite directions is even more explicit in WAV.CUR_STA (Figure 9c), where the vorticity to the northeast of the cyclone is stronger in comparison to WAV.CUR. When the surface currents are smoothed in WAV.CUR_LOW, most of the mesoscale energy is suppressed and the resulting vorticity is much weaker in comparison with WAV.CUR and WAV.CUR_STA. As a consequence, there is no significant refraction, and the significant wave height is nearly uniform in the azimuthal direction.

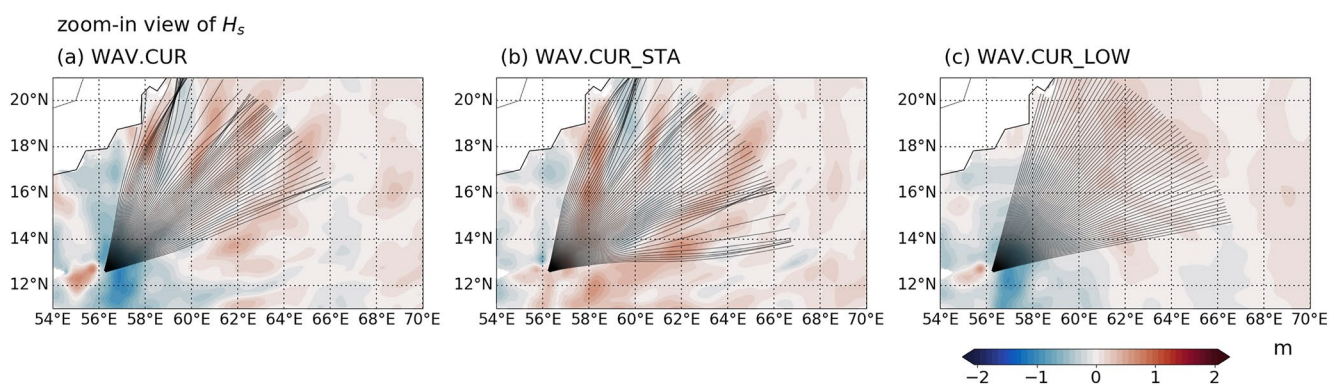

Figure 8. Ray-tracing analysis of the waves generated from the eyewall of the tropical cyclone on May 24. Panels (a–c) show ray-tracing analysis results superimposed for WAV.CUR, WAV.CUR_STA, and WAV.CUR_LOW, respectively. The background contours indicate H_s obtained from WAV.CUR, WAV.CUR_STA, and WAV.CUR_LOW in comparison with WAV.WND.

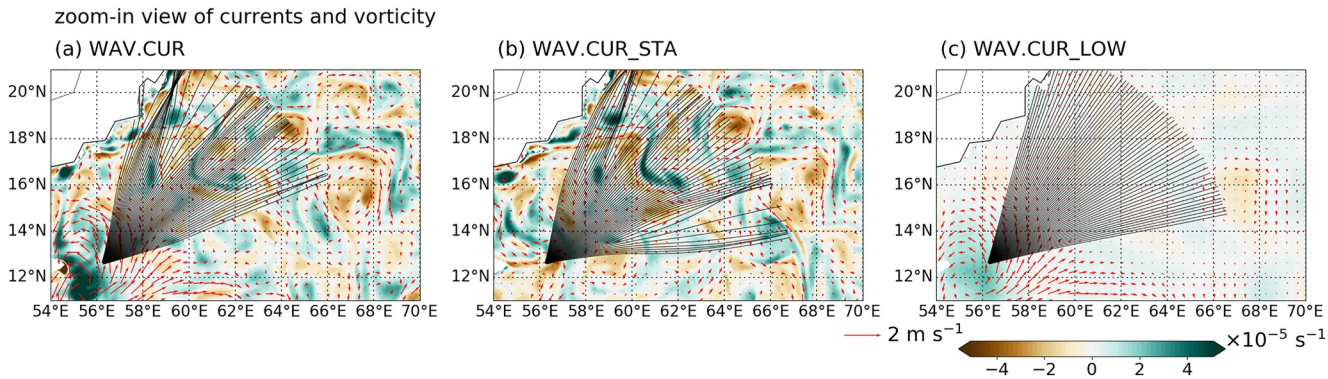

Figure 9. Ray-tracing analysis plotted on top of the vorticity and currents. Panels (a–c) show ray-tracing analysis results for WAV.CUR, WAV.CUR_STA, and WAV.CUR_LOW, respectively.

4. Discussion

Recent observational and modeling studies have highlighted the importance of wave-current interactions in determining the sea state. In particular, these studies suggest that at oceanic meso- and submesoscales the spatial gradients in the significant wave height field arise from focusing and defocusing of wave action due to refraction by ocean currents (Ardhuin et al., 2017; Marechal & Ardhuin, 2021; Villas Bôas et al., 2020). To better understand the impact of currents on tropical-cyclone generated waves, here we used a regional wave model to show that including mesoscale currents in a tropical cyclone simulation leads to alternating regions of high and low H_s starting near the eyewall and extending to the northeast all the way to 100 m isobath. The spatial variability in H_s observed in the model simulations is consistent with the available altimeter data (the RMS difference between WAV.CUR and altimeter data is 0.37 m), and reveals ocean current-driven variations in H_s up to approximately 2 m (e.g., on 25th May, H_s varies from 1.9 to 3.9 m between 20° and 25°N from SARAL/Altika data).

Wave ray-tracing through the ocean currents gives understanding of the observed patterns of focusing and defocusing of wave energy and the resulting H_s structure. Although one previous study focused on the effects of cyclone-induced surface currents on the sea state (Fan, Ginis, & Hara, 2009), both our WW3 simulations and ray-tracing analysis suggest that the spatial gradients in H_s are dominated by the background currents and are not significantly influenced by the tropical cyclone induced currents. Importantly, this simplifies the problem of predicting these wave state gradients. The existing background cyclonic and anticyclonic eddies cause the cyclone induced rays to bend in opposite directions, creating regions of high and low ray concentration. The strength of eddy vorticity leads to stronger refraction (higher ray curvature). This is demonstrated here by comparing ray trajectories using fully resolved currents (WAV.CUR) and smoothed currents (WAV.CUR_LOW); when the spatial variability of the currents is suppressed the eddies are not strong enough to cause significant deflections in the ray trajectories and regions of amplified H_s are not simulated. Here, we show that including ocean surface current forcing in the wave model leads to spatial gradients of H_s that better correlate with altimetry observations. It is possible that small spatiotemporal-scale winds not resolved by ERA5 could also affect the observed structure in H_s. Future work should assess the relative impact of high-frequency, high-wavenumber wind variability, and ocean currents on surface ocean wave variability.

Waves provide much of the energy driving coastal and beach erosion, flooding, and wave overtopping (Young et al., 2021), making accurate wave modeling of paramount importance for adaptation and mitigation efforts in response to extreme events. Although there has been significant improvement in weather and wave forecasting systems, most operational wave models exclude current forcing (Ardhuin et al., 2012). This paper demonstrates that background mesoscale currents affect cyclone-generated waves, leading to spatial gradients in the significant wave height. Importantly, for some regions the currents amplify the wave heights by 1 m. Although we focused the discussion on Cyclone Mekunu, the same spatial pattern of amplified and diminished beams of H_s was observed during other tropical cyclones (see Supporting Information S1). This suggests the findings here are a general feature of tropical-cyclone-generated waves in the Arabian Sea due to interactions with background currents. Variations in the total water level represent a major hazard for densely populated coastal areas. The contribution of surface waves to the total water level can be generally parameterized as a function of the offshore significant

wave height and period (Dodet et al., 2019). Here, we have shown that when the effects of currents are not taken into account the modeled wave heights at some major cities on the Arabian Sea coast can be underestimated by up to 1 m. This translates into a significant underestimation of the wave-driven contribution to the total water level and presents a clear risk to the coastal population.

Conflict of Interest

The authors declare no conflicts of interest relevant to this study.

Data Availability Statement

The simulation results are available at: https://doi.org/10.5281/zenodo.4660321. We used WAVEWATCH III version 5.16 compiled with the following switches: F90 NOGRB NOPA LRB4 SCRIP SCRIPNC NC4 TRKNC DIST MPI PR3 UQ FLX0 LN1 ST4 STAB0 NL1 BT4 DB1 MLIM TR0 BS0 IC2 IS2 REF1 IG0 XX0 WNT2 WNX1 RWND CRT1 CRX1 TIDE O0 O1 O2 O2a O2b O2c O3 O4 O5 O6 O7.

Acknowledgments
The authors gratefully acknowledge the research funding (grant number: OSR-2-16-RPP-3268.02) from KAUST (King Abdullah University of Science and Technology). The authors also appreciate the computational resources related to the supercomputer Shaheen II and the assistance provided by KAUST Supercomputer Laboratory. Ana B. V. Bôas was funded by the SWOT program with NASA grants NNX16AH67G and 80NSSC20K1136. Bruce D. Cornuelle, Matthew R. Mazloff, and Aneesh C. Subramanian acknowledge funding from NOAA awards NA21OAR4310257, NA18OAR4310403, NA18OAR4310405. The authors wish to thank Fabrice Ardhuin for discussing the simulation results and the setup of the numerical simulations.

References

Abolfazli, E., Liang, J.-H., Fan, Y., Chen, Q. J., Walker, N. D., & Liu, J. (2020). Surface gravity waves and their role in ocean-atmosphere coupling in the Gulf of Mexico. *Journal of Geophysical Research: Oceans*, *125*(7), e2018JC014820. https://doi.org/10.1029/2018jc014820

Alday, M., Accensi, M., Ardhuin, F., & Dodet, G. (2021). A global wave parameter database for geophysical applications. Part 3: Improved forcing and spectral resolution. *Ocean Modelling*, *166*, 101848. https://doi.org/10.1016/j.ocemod.2021.101848

Ardhuin, F., Gille, S. T., Menemenlis, D., Rocha, C. B., Rascle, N., Chapron, B., et al. (2017). Small-scale open ocean currents have large effects on wind wave heights. *Journal of Geophysical Research: Oceans*, *122*(6), 4500–4517. https://doi.org/10.1002/2016jc012413

Ardhuin, F., Roland, A., Dumas, F., Bennis, A.-C., Sentchev, A., Forget, P., et al. (2012). Numerical wave modeling in conditions with strong currents: Dissipation, refraction, and relative wind. *Journal of Physical Oceanography*, *42*(12), 2101–2120. https://doi.org/10.1175/jpo-d-11-0220.1

Booij, N., & Holthuijsen, L. H. (1987). Propagation of ocean waves in discrete spectral wave models. *Journal of Computational Physics*, *68*(2), 307–326. https://doi.org/10.1016/0021-9991(87)90060-x

Cavaleri, L., Fox-Kemper, B., & Hemer, M. (2012). Wind waves in the coupled climate system. *Bulletin of the American Meteorological Society*, *93*(11), 1651–1661. https://doi.org/10.1175/bams-d-11-00170.1

Chassignet, E. P., Hurlburt, H. E., Smedstad, O. M., Halliwell, G. R., Hogan, P. J., Wallcraft, A. J., & Bleck, R. (2007). The HYCOM (hybrid coordinate ocean model) data assimilative system. *Journal of Marine Systems*, *65*(1–4), 60–83. https://doi.org/10.1016/j.jmarsys.2005.09.016

Chen, S. S., Zhao, W., Donelan, M. A., & Tolman, H. L. (2013). Directional wind–wave coupling in fully coupled atmosphere–wave–ocean models: Results from CBLAST-Hurricane. *Journal of the Atmospheric Sciences*, *70*(10), 3198–3215. https://doi.org/10.1175/jas-d-12-0157.1

Dodet, G., Melet, A., Ardhuin, F., Bertin, X., Idier, D., & Almar, R. (2019). The contribution of wind-generated waves to coastal sea-level changes. *Surveys in Geophysics*, *40*(6), 1563–1601. https://doi.org/10.1007/s10712-019-09557-5

Drost, E. J. F., Lowe, R. J., Ivey, G. N., Jones, N. L., & Péquignet, C. A. (2017). The effects of tropical cyclone characteristics on the surface wave fields in Australia's North West region. *Continental Shelf Research*, *139*, 35–53. https://doi.org/10.1016/j.csr.2017.03.006

Dube, S. K., Rao, A. D., Sinha, P. C., Murty, T. S., & Bahulayan, N. (1997). Storm surge in the Bay of Bengal and Arabian Sea the problem and its prediction. *Mausam*, *48*(2), 283–304.

Dysthe, K. B. (2001). Refraction of gravity waves by weak current gradients. *Journal of Fluid Mechanics*, *442*, 157–159. https://doi.org/10.1017/s0022112001005237

Evan, A. T., & Camargo, S. J. (2011). A climatology of Arabian Sea cyclonic storms. *Journal of Climate*, *24*(1), 140–158. https://doi.org/10.1175/2010jcli3611.1

Evan, A. T., Kossin, J. P., Ramanathan, V., & Ramanathan, V. (2011). Arabian Sea tropical cyclones intensified by emissions of black carbon and other aerosols. *Nature*, *479*(7371), 94–97. https://doi.org/10.1038/nature10552

Fan, Y., Ginis, I., & Hara, T. (2009). The effect of wind–wave–current interaction on air–sea momentum fluxes and ocean response in tropical cyclones. *Journal of Physical Oceanography*, *39*(4), 1019–1034. https://doi.org/10.1175/2008jpo4066.1

Fan, Y., Ginis, I., Hara, T., Wright, C. W., & Walsh, E. J. (2009). Numerical simulations and observations of surface wave fields under an extreme tropical cyclone. *Journal of Physical Oceanography*, *39*(9), 2097–2116. https://doi.org/10.1175/2009jpo4224.1

Hegermiller, C. A., Warner, J. C., Olabarrieta, M., & Sherwood, C. R. (2019). Wave–current interaction between hurricane Matthew wave fields and the Gulf Stream. *Journal of Physical Oceanography*, *49*(11), 2883–2900. https://doi.org/10.1175/jpo-d-19-0124.1

Hersbach, H., Bell, B., Berrisford, P., Hirahara, S., Horányi, A., Muñoz-Sabater, J., et al. (2020). The ERA5 global reanalysis. *Quarterly Journal of the Royal Meteorological Society*, *146*(730), 1999–2049.

Holthuijsen, L. H., & Tolman, H. L. (1991). Effects of the Gulf Stream on ocean waves. *Journal of Geophysical Research: Oceans*, *96*(C7), 12755–12771. https://doi.org/10.1029/91jc00901

Kenyon, K. E. (1971). Wave refraction in ocean currents. *Deep Sea Research and Oceanographic Abstracts*, *18*(10), 1023–1034. https://doi.org/10.1016/0011-7471(71)90006-4

Liu, Q., Babanin, A., Fan, Y., Zieger, S., Guan, C., & Moon, I.-J. (2017). Numerical simulations of ocean surface waves under hurricane conditions: Assessment of existing model performance. *Ocean Modelling*, *118*, 73–93. https://doi.org/10.1016/j.ocemod.2017.08.005

Marechal, G., & Ardhuin, F. (2021). Surface currents and significant wave height gradients: Matching numerical models and high-resolution altimeter wave heights in the agulhas current region. *Journal of Geophysical Research: Oceans*, *126*(2), e2020JC016564. https://doi.org/10.1029/2020jc016564

Mogensen, K. S., Magnusson, L., & Bidlot, J.-R. (2017). Tropical cyclone sensitivity to ocean coupling in the ECMWF coupled model. *Journal of Geophysical Research: Oceans*, *122*(5), 4392–4412. https://doi.org/10.1002/2017jc012753

Munk, W. H., & Traylor, M. A. (1947). Refraction of ocean waves: A process linking underwater topography to beach erosion. *The Journal of Geology*, *55*(1), 1–26. https://doi.org/10.1086/625388

Murakami, H., Vecchi, G. A., & Underwood, S. (2017). Increasing frequency of extremely severe cyclonic storms over the Arabian Sea. *Nature Climate Change*, *7*(12), 885–889. https://doi.org/10.1038/s41558-017-0008-6

Olabarrieta, M., Warner, J. C., Armstrong, B., Zambon, J. B., & He, R. (2012). Ocean–atmosphere dynamics during hurricane Ida and Nor'Ida: An application of the coupled ocean–atmosphere–wave–sediment transport (COAWST) modeling system. *Ocean Modelling*, *43*, 112–137. https://doi.org/10.1016/j.ocemod.2011.12.008

Phillips, O. M. (1977). *The dynamics of the upper ocean* (2nd ed.). Cambridge University Press.

Prakash, K. R., & Pant, V. (2020). On the wave-current interaction during the passage of a tropical cyclone in the Bay of Bengal. *Deep Sea Research Part II: Topical Studies in Oceanography*, *172*, 104658. https://doi.org/10.1016/j.dsr2.2019.104658

Queffeulou, P., & Croizé-Fillon, D. (2013). *Global altimeter SWH data set, version 10. (Tech. Rep.)*. Laboratoire d'Océanographie Spatiale, IFREMER. Retrieved from https://fr/ifremer/cersat/products/swath/altimeters/waves/

Quilfen, Y., & Chapron, B. (2019). Ocean surface wave-current signatures from satellite altimeter measurements. *Geophysical Research Letters*, *46*(1), 253–261. https://doi.org/10.1029/2018gl081029

Quilfen, Y., Yurovskaya, M., Chapron, B., & Ardhuin, F. (2018). Storm waves focusing and steepening in the Agulhas current: Satellite observations and modeling. *Remote Sensing of Environment*, *216*, 561–571. https://doi.org/10.1016/j.rse.2018.07.020

Rascle, N., & Ardhuin, F. (2013). A global wave parameter database for geophysical applications. Part 2: Model validation with improved source term parameterization. *Ocean Modelling*, *70*, 174–188. https://doi.org/10.1016/j.ocemod.2012.12.001

Romero, L., Hypolite, D., & McWilliams, J. C. (2020). Submesoscale current effects on surface waves. *Ocean Modelling*, *153*, 101662. https://doi.org/10.1016/j.ocemod.2020.101662

Tolman, H. L. (2002). Alleviating the garden sprinkler effect in wind wave models. *Ocean Modelling*, *4*(3–4), 269–289. https://doi.org/10.1016/s1463-5003(02)00004-5

Villas Bôas, A. B., Ardhuin, F., Ayet, A., Bourassa, M. A., Brandt, P., Chapron, B., et al. (2019). Integrated observations of global surface winds, currents, and waves: Requirements and challenges for the next decade. *Frontiers in Marine Science*, *6*, 425. https://doi.org/10.3389/fmars.2019.00425

Villas Bôas, A. B., Cornuelle, B., Mazloff, M., Gille, S., & Ardhuin, F. (2020). Wave–current interactions at meso-and submesoscales: Insights from idealized numerical simulations. *Journal of Physical Oceanography*, *50*(12), 3483–3500. https://doi.org/10.1175/jpo-d-20-0151.1

Warner, J. C., Armstrong, B., He, R., & Zambon, J. B. (2010). Development of a coupled ocean–atmosphere–wave–sediment transport (COAWST) modeling system. *Ocean Modelling*, *35*(3), 230–244. https://doi.org/10.1016/j.ocemod.2010.07.010

WAVEWATCH III Development Group. (2016). User manual and system documentation of WAVEWATCH III version 5.16. NOAA/NWS/NCEP/MMAB Technical Note, 329, 326.

Young, A. P., Guza, R. T., Matsumoto, H., Merrifield, M. A., O'Reilly, W. C., & Swirad, Z. M. (2021). Three years of weekly observations of coastal cliff erosion by waves and rainfall. *Geomorphology*, *375*, 107545. https://doi.org/10.1016/j.geomorph.2020.107545